Iranica Journal of Energy & Environment
Journal Homepage: www.ijee.net
IJEE an official peer review journal of Babol Noshirvani University of Technology, ISSN:2079-2115

Reduction of Metal Artifact in Dental Computed Tomography by Homomorphic Wavelet Filtering in Sinogram Domain

H. Hassanpour[1]*, R. Ebadi[1], A. Zehtabian[2] and Z. Amiri[1]

[1] *Faculty of Computer Engineering, Shahrood University of Technology, Shahrood, Iran*
[2] *Institute for Chemistry and Biochemistry, Free University of Berlin, Berlin, Germany*

P A P E R I N F O

Paper history:
Received 06 December 2018
Accepted in revised form 31 December 2018

Keywords:
Metal artifact reduction
Illumination-reflectance model
Homomorphic wavelet filtering
Sinogram domain
Dental X-ray images

A B S T R A C T

In X-ray computed tomography (CT), existence of metallic implants in the subject may corrupt images and produce dark and bright streaking artifacts. In this paper a new method for reducing metal artifact from dental X-ray CT images is introduced. In the proposed method, the Radon transform is used in order to project the CT data into the sinogram domain. The sinogram of data can be decomposed into its illumination and reflectance components by using the homomorphic wavelet filtering. The investigation of the CT images shows that the degradations caused by metallic artifacts appear mainly in the illumination component. Therefore, in our approach the corrupted illumination component is restored by using the apriori information driven from the previous artifact-free sections. The results showed that the metal artifacts are considerably reduced without eliminating the important details of the CT images. The proposed method is also compared with other existing methods on a set of dental CT images. Comparisons showed the superiority of the proposed method over other existing methods.

***doi**: 10.5829/ijee.2018.09.04.06*

INTRODUCTION

Computed Tomography (CT) is one of the most useful imaging procedures in medical imaging [1,2, 3]. CT uses X-ray radiation in order to create detailed scans of the body's internal organs. In this technology, the X-ray beams propagate from different angles through the area of interest into the patient's body in order to provide a cross-sectional image. CT detectors then record those X-rays which are not completely attenuated during the transmission through the organs of the patient [4].

One of the major challenges in CT imaging is the presence of artifacts caused by metallic implants which are surgically implanted in the body of patients [5]. In comparison to biological tissues, the metallic implants have a higher cross section for X-rays attenuation. As a consequence, when a given X-ray reaches the implant, its attenuation level increases. Therefore, fewer number of photons can reach the detectors. It leads to serious corruptions in the CT images, especially near the metal surfaces [6,7]. When a given image is corrupted by the metal artifact, the areas in front and behind a metallic object contain the bright and the dark streaks, respectively. These streaks dramatically affect the quality of the CT data and lead to improper interpretation of the results. CT images are often provided as separate stacked 2D slices. Since the metallic inserts usually occupy a relatively little space, only a small number of slices are prone to be corrupted by metallic implants [8]. Therefore, one solution for reconstructing the corrupted slices is to utilize a priori knowledge that can be extracted from the adjacent non-corrupted slices. The left-hand column in Figure 1 shows two different slices of a CT data taken from the teeth of a patient with a metal implant.

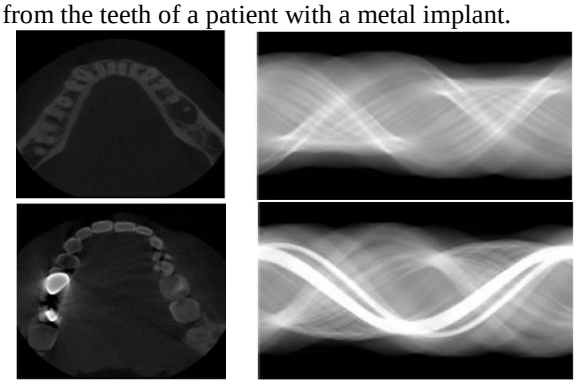

Figure1. Two different slices of a dental CT. Images in the left-hand column are represented in spatial domain, while the right-hand ones are their representations in sinogram domain. Only the second slice is affected by metal artifacts.

* Corresponding author: Hamid Hassanpour
E-mail: h_hassanpour@yahoo.com

The right-hand column shows their corresponding sinogram. The sinogram representation of an image is composed of sets of line integrals of that image along straight lines in various angles [9, 10]. The degradations caused by the metallic implants are more difficult to be reduced through using traditional noise/artifact reduction scenarios [11,12,13] that mainly focus on removing background noises. The most widely-used methods dealing with metal artifact reduction can be roughly categorized into two groups: the projection completion techniques [3.14], and the iterative reconstruction algorithms [6,8]. In the projection completion-based methods, the corrupted data are restored using various types of restoration techniques such as linear/polynomial interpolations. In the iterative approach, the corrupted data is reconstructed by some iterative tools such as maximum likelihood estimation maximization or algebraic reconstruction techniques[3]. Applying the iterative methods may result in better reconstructions. However, the process often needs a considerably higher computational time [15,16].

A two-step metal artifact reduction algorithm is proposed in this paper. The algorithm is based on homomorphic wavelet filtering which is carried out in the sinogram domain. Compared to most of the other competing methods, the proposed method is straight-forward and reduces the effects of metal artifacts without degrading the CT image quality. Moreover, it does not rely on any additional pre-processing step such as segmentation or noise reduction. The rest of the paper is organized as follow: section 2 gives a brief overview of related works. The proposed methodology is described in section 3. In section 4, the experimental results are presented. Finally, in section 5, conclusions of the study are drawn.

Literature review

As mentioned before, the existing metal artifact reduction methods can be categorized into the projection completion techniques and the iterative image reconstruction algorithms. In continue, some of these methods are reviewed. A dynamic wavelet thresholding metal artifact reduction algorithm was produced by Peng et al. [17], which is based on a statistic iterative reconstruction model for CT images. For removing blocky black artifacts caused by incomplete projections, cubic spline interpolation was utilized. A modified mean-shift segmentation was used for reducing the metal artifacts [7]. After projecting the image into the sinogram domain, the authors delete the corrupted projection from the original projection and then benefit from the feedback interpolation strategy in order to produce a new interpolation projection. Finally, they reconstruct the artifact-reduced image using a traditional backward projection technique [7].

De Crop *et al.* [18] and Wagenaar *et al.* [12] evaluated several metal artifact reduction methods used in dental CT images and reported their advantageous and drawbacks. Using the known geometry of the boundaries of the high-attenuation objects in CT data, researchers analyzed the data and performed the artifact reduction procedure [19]. To this end, they segment the metallic objects and then detect the position and orientation of the rigid objects. An automatic approach for segmentation of dental CT images was proposed by Mortaheb and Rezaeian [20], in which a preprocessing step (based on least square support vector machines) was exploited to reduce the metal artifacts. Nasirudin et al. [13] showed the efficiency of combining some additional information taken from Spectral CT (SCT) with the traditional statistical based reconstruction methods in improving the metal artifact reduction level. Johari et al. [21] introduced an artifact reduction algorithm with three parallel components. The teeth are extracted based on modeling the image histogram with a Gaussian mixture model in the first component. Streaking artifact components are reduced using morphological filtering by converting image into the polar domain. The cavities are filled using a morphological filtering operation performed by the third component.

There are several approaches in the sinogram domain to overcome the metal artifact phenomenon [3, 22]. Such approaches are mainly based on detecting the mismatches between the measured sinogram data and the ideal forward projectors [19]. To this end, metal objects are first segmented using thresholding techniques. Then forward projection is applied to obtain the corresponding sinograms. After normalizing the sinograms, the interpolation techniques are used in order to reconstruct the degraded sinograms and consequently restore the corrupted CT data [22]. Although the sinogram-based methods are usually capable of reducing the artifacts, their main disadvantage is the high dependency of the results on the segmentation performance [22]. An inaccurate segmentation of the metal objects often leads to an inappropriate detection of corrupted regions in the image [22].

Proposed method

The proposed approach consists of two steps. In the first step, the retrieval process is implemented in a sequential manner. As discussed in our previous work [23], various types of image impairments have different effects on its illumination and reflectance components. In cases in which the impairments are caused by the metal implants, the illumination component is more affected in comparison with the reflectance component. Hence, at first the CT images are transformed into the sinogram domain, then their illumination-reflectance components are extracted. The illumination component of a given corrupted sinogram is then substituted with the illumination component of the artifact-free sinogram

associated with its closest prior section. By combining the reconstructed illumination component with the reflectance component, the enhanced sinogram is obtained. In this step, therefore, the reconstruction process is applied to the corrupted sinogram as a whole. In the second step, the reconstruction process is more localized in the sense that it specifically affects such regions in the corrupted sinogram which are more likely to be degraded by the metal artifacts.

Step 1: sequential reconstruction

A sequential reconstruction methodology is proposedin the first step of the approach. In this step, all available CT slices are first transformed into sinogram domain. The process of transforming an image into the corresponding sinogram is called forward-projection (FP). Afterward, in order to reduce the metal artifacts in a given corrupted section, the sinogram of the nearest precedent section which seems to be not much affected by the metal artifacts is used as a priori knowledge for restoring the corrupted section. As discussed in literature [10], an image can be modeled as a combination of two components: the illumination and the reflectance (Equation 1), where the former stands for the illumination properties of the scene and the latter deals with the reflectance levels related to the objects within the scene.

$$f(x,y) = r(x,y) \times e(x,y) \quad (1)$$

From the frequency point of view, the illumination component contains lower frequency components of the image (i.e. slower changes in the intensities of pixels) [10]. In contrary, the reflectance component mainly contains higher frequency components of the image [10]. After applying the artifact reduction technique to the corrupted sinograms, the inverse sinogram transform should be done to get back to the original spatial domain. In this paper, one of the most widely used inverse transforms (i.e. filtered-back-projection or FBP) is applied, which has been exploited by Kak [24].

As mentioned before various types of impairments have different effects on the illumination and reflectance components, and the metal implants impairments affect the illumination component overthan the reflectance component. Our recent studies show that this difference is more obvious in the sinogram domain than the spatial domain. Homomorphic filtering is a useful tool for projecting an image into its corresponding illumination-reflectance model because it can control both high frequency and low frequency components of an image via selection of an appropriate filtering function. The homomorphic filters mainly map the linear filtering approaches to a different domain and then map them back to the original domain [10]. In the presented research, we used the wavelet-based version of homomorphic filtering in which the wavelet analysis is chosen to act as the principal filter in homomorphic domain. Figure 1 outlines the details of the procedure. As can be seen, the sinogram of each slice ($i.e.\ (x,y)$) is first fed into the algorithm. In order to replace the multiplication operation in Equation 1 by the summation operation, a logarithm function is applied to $f(x,y)$. Therefore, Equation 2 can be updated to Equation 3. As a result, the two components can be separated easier, since the reflectance component can now be achieved by subtracting the illumination component from $f(x,y)$, but in the logarithmic domain.

$$ln\, f(x,y) = ln\, r(x,y) + ln\, e(x,y) \quad (2)$$

Using the homomorphic-wavelet procedure, the illumination-reflectance components of the sinograms corresponding to all the CT slices are achieved. In a given corrupted sinogram (i.e. $P^c_{(n)}(\rho,s)$), its illumination component is substituted with that of the closest precedent artifact-free sinogram (i.e. $e^{a-f}_{(1\le m<n)}(\rho,s)$). After combining this illumination component with the reflectance component of the corrupted sinogram (i.e. $r^c_{(n)}(\rho,s)$) using the inverse homomorphic filtering, the initial artifact-reduced sinogram is achieved, as described in Equation 2:

$$\hat{P}^c_{(n)}(\rho,s) = e^{a-f}_{(1\le m<n)}(\rho,s) \times r^c_{(n)}(\rho,s) \quad (3)$$

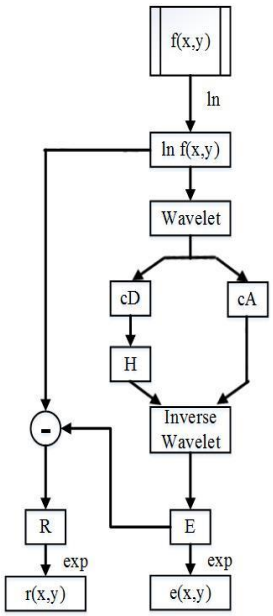

Figure 1. Block-diagram of the homomorphic-wavelet filtering technique used in the proposed method: $f(x,y)$ = input data (i.e. the sinogram of each slice of the CT image), cA = approximation coefficients, cD = detail coefficients in vertical/ horizontal/diagonal directions, H = Gaussian filter, E = illumination component in logarithmic domain, R = reflectance component in logarithmic domain, $e(x,y)$ and $r(x,y)$ = final illumination and reflectance components of the input sonogram.

After replacing the corrupted sinogram with the artifact-reduced sinogram, the sequential (forward) reconstruction process continues to the next corrupted sinograms, if any. The reconstructed CT data are achieved after all corrupted sinograms (corresponding to all corrupted sections) were processed using the proposed method.

Step 2: weighted reconstruction

We only need to enhance the disturbed area of the image as the whole image may not be affected by the metal artifact. In other words, the undamaged area is masked from the reconstruction process. Therefore, we propose to extract a nonlinear sinogram mask $P_{(n)}^{mask}(\rho, s)$from the corrupted sinogram$P_{(n)}^{c}(\rho, s)$. To this end, one threshold value (T) is defined as the average of $P_{(n)}^{c}(\rho, s)$. Then the region in the corrupted sinogram with values larger than the threshold are extracted. After normalizing the extracted areas, to keep them between 0 and 1, the result is considered as the nonlinear sinogram mask $P_{(n)}^{mask}(\rho, s)$. The nonlinear mask is then used as a weighting factor in order to combine the two sinograms: the corrupted sonogram $P_{(n)}^{c}(\rho, s)$, and the corresponding initially reconstructed sinogram $\hat{P}_{(n)}^{c}(\rho, s)$ which has been achieved using the first step of the proposed algorithm. In Equation 4 the final reconstructed sinogram $P_{(n)}^{final}(\rho, s)$ is obtained.

$$P_{(n)}^{final}(\rho, s) = P_{(n)}^{mask}(\rho, s) \times \hat{P}_{(n)}^{c}(\rho, s) + \left(1 - P_{(n)}^{mask}(\rho, s)\right) \times P_{(n)}^{c}(\rho, s) \quad (4)$$

The reconstructed sinograms are then transferred back into the spatial domain by the inverse sinogram transform and the artifact-reduced CT images are finally achieved. As will be discussed in the next section, the artifacts caused by the metallic implants are considerably reduced, while the artifact-free regions are not affected by the proposed reconstruction procedure.

RESULTS AND EVALUATION

The performance evaluation of the proposed approach as well as some of the competing artifact reduction methods are presented in this section. For this purpose, they have been applied to several data taken from a dataset containing a series of 930 real dental CT images among which 341 images are affected by the metal implants. This dataset has been acquired at the Face and Jaw Radiography Center (FJRC), Babol, Iran. All the CT sections shown in the figures of the present paper have been selected from this real clinical dataset.

At first, in order to visually show the effects of the metal artifacts on the illumination and reflectance components in the sinogram domain, we apply the homomorphic-wavelet filtering to the sinogram representations of two sections of a dental CT data (Figure 2). As you can see, one of the two sections is not affected by metal artifact(Figure 2-a). After separating the illumination and reflectance components in the sinogram domain (Figure 2-b), each of them is projected back to the spatial domain using the inverse sinogram transform (Figure 2-c).

Moreover, the visual results of applying the first step of the proposed reconstruction algorithm to the two given corrupted sinograms are illustrated in Figure 3. This figure clearly shows that the artifacts have been considerably reduced using the first step. Nevertheless, after a careful analysis of the results, it can be deduced that some other useful details such as the textural details of the frontal teeth are eliminated in the reconstructed sections. This drawback can be overcome by applying the second step of the proposed artifact reduction algorithm because this outcome is caused by substituting the degraded illumination component as a whole which leads to information loss and consequently results in some unwanted effects in the final results, and the second step is a solution to this problem. The results of applying the second step of the proposed method are shown in Figure 5. As can be inferred from this figure, the metal artifacts are considerably reduced, while the artifact-free regions are not affected by the reconstruction procedure.

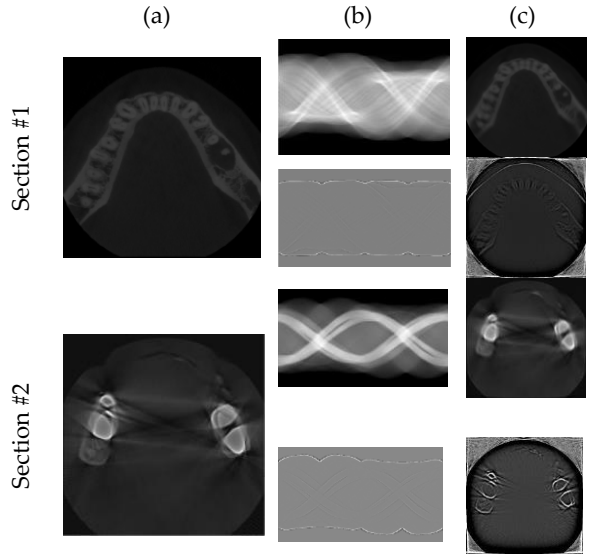

Figure 2. Effects of metal artifacts on the illumination and reflectance components: (a) two CT sections; (b) from top to bottom respectively, the corresponding illumination and reflectance components in the sinogram domain; (c) from top to bottom respectively, the results of projecting the illumination and reflectance components back to the spatial domain.

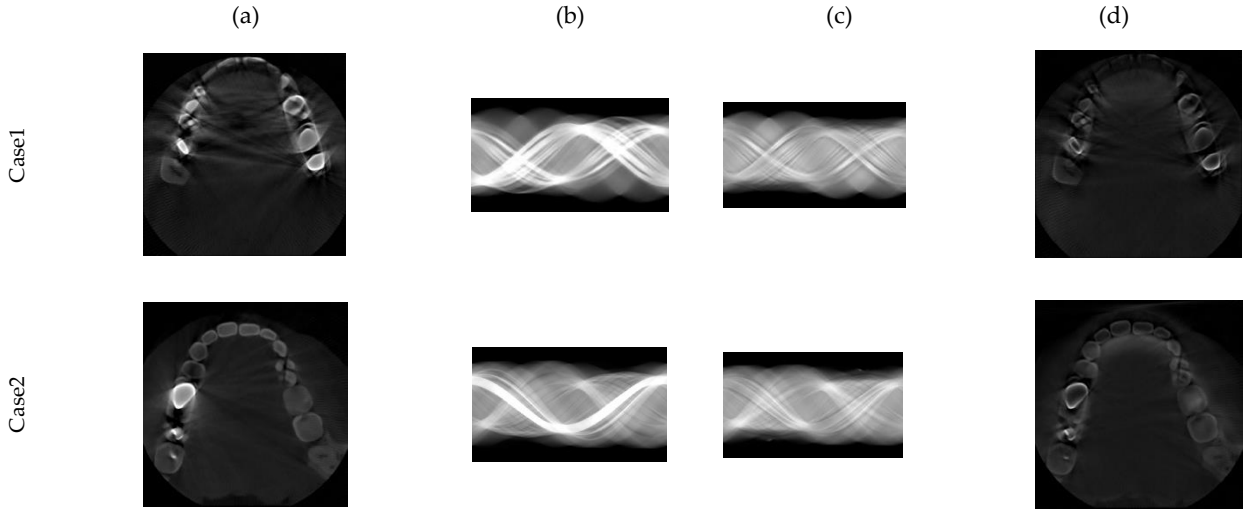

Figure 3. Applying the first step of the proposed approach on two different corrupted sinograms affected by metal artifacts. (a) two CT sections. (b) sinograms corresponding to slices. (c) the result of combining the IC-NPNSs and the RC-CSs in order to produce the reconstructed sinogram achieved by the first step of the proposed method. (d) The spatial domain representations of the reconstructed sinograms.

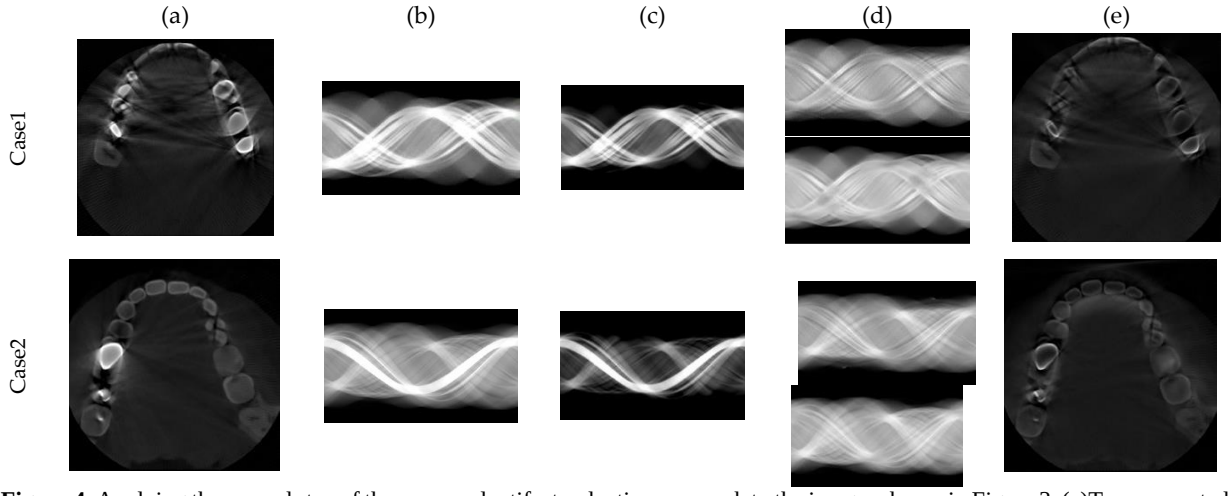

Figure 4. Applying the second step of the proposed artifact reduction approach to the images shown in Figure 3. (a)Two corrupted images. (b) Sinograms corresponding to the slices. (c) The nonlinear sinogram masks extracted from the corrupted sinograms (d) From top to bottom,results of the first step of the proposed approach, the final reconstructed sinograms after applying the second step of the proposed approach. (e) Final results of the proposed approach.

Finally, we follow an application-based quantitative evaluation in order to provide a comparison between the proposed method and three other artifact-reduction approaches [5], [19] [20]] by using the corrupted and artifact-reduced clinical data as well as their corresponding reference ground truth maps defined on uncorrected images. To this end, 20 dental CT images which have been corrupted by metal artifacts are randomly chosen from the database of the Face and Jaw Radiography Center. Due to absence of predefined ground truths for the utilized data, one corrupted slice is randomly selected from each CT image as a candidate and its ground truth is manually generated by the expert radiologists of FJRC. In this experiment scenario, the ground truths are two-class maps in which the teeth and non-teeth tissues (i.e. soft tissues, air, bone, etc.) are distinguished. These maps are later used as references for further evaluations.

A two-class Support Vector Machine (SVM) classifier is utilized for classifying the pixels of each candidate corrupted slice as well as its artifact-reduced versions. The pixels are supposed to be classified into two classes: teeth and non-teethafter applying the proposed approach and the three other competing

methods to the selected dental CT images. To this end, the SVM classifier should be first trained. In our experiments, 10% of the available pixels of each class are used as the training samples. These samples have been randomly selected from the reference grand truths. After training the classifier, all the candidate corrupted slices and artifact-reduced slices are classified. To be more clear, each pixel of the 20 corrupted slices and 80 artifact-reduced slices (i.e. four artifact-reduced versions of each corrupted slice) are labeled as one of the two classes.

The classification accuracies and reliabilities after applying the SVM classifier to the examined data are the quantitative measures used in this experiment. In our evaluations, the percentage of the true teeth pixels which are correctly classified to the teeth class according to the reference class mapis defined asthe classification accuracy. Meanwhile, the classification reliability is defined as the ratio between the number of pixels that are correctly classified as teeth, and all the pixels which are correctly/incorrectly classified to the teeth class. These two measures are expressed in percent. In an ideal teeth classification (when the both measures are in their maximum value, i.e. %100), all the true teeth pixels are correctly labeled as teeth class, while there is no non-teeth pixel which is classified as teeth.

Furthermore, in order to simplify the comparisons, since only two reference classes are considered in our implementation(i.e. teeth and non-teeth), we only report the classification rations of the teeth class (see TABLE 1). It is also worth noting that the classification ratios achieved for all the 20 corrupted data are first averaged and then drawn in the table. Accordingly, for further evaluations, the standard deviations of the gained results are also reported. Moreover, using the same training sets for each candidate slice, can guarantee a fair comparison between the results of applying the four methods. Finally, the implementation of the SVM classifier is based on using an online available package named as 'A Library for Support Vector Machines' (LIBSVM) [25]. In the SVM implementation, a Gaussian kernel is used whose parameters are tuned using five folds cross validation.

As can be seen in TABLE 1, all the artifact reduction methods can properly reduce the effects of metal artifacts and consequently enhance the classification performance. Among the competing methods, the one proposed in literature [5] showed the best performance in term of classification accuracy, since it increases the average accuracy from 66.55 to 81.22%. The second rank belongs to the method presented by Park et al. [19] while our proposed approach is third-order accurate. In term of classification reliability, however, our method gives the best performance. To be more clear, the proposed method results in a lower false positive detection rate compared to the other competing techniques.

TABLE 1. Performance comparison between the proposed method and the three competing artifact reduction approaches. Average classification accuracies and reliabilities (in percent) as well as the standard deviations (S.D) of the gained results are reported for 20 corrupted dental CT slices before and after applying the artifact reduction methods

Method	Proposed Method	Wavelet-Domain Sparse Regularization [5]	Beam-Hardening Corrector [19]	Least Square Support Vector Machine and Mean Shift Algorithm [20]
Classification Accuracy (± S.D)	% 77.96 ± % 4.02	% 81.22 ± % 3.76	% 79.61 ± % 2.72	% 70.08 ± % 4.33
Classification Reliability (± S.D)	% 75.87 ± % 3.61	% 72.14 ± % 3.97	% 66.80 ± % 3.07	% 63.12 ± % 4.60

It is mainly because of this fact that the proposed two-step sinogram reconstruction algorithm is considerably successful in reducing the bright streak artifacts. From the classification reliability point of view, the method introduced by Mehranian et al. [5] has the second rank.

The proposed method is compared from the computational complexity by using an Intel core i5-6200u CPU at 2.3 GHz with 8 Gbytes of memory. Our approach performed better than the other three methods except the one which was based on wavelet-domain sparse regularization [5]. The average time needed for applying the proposed approach to 20 corrupted dental CT slices was five minutes and 351 seconds. For the proposed method [5], it took less than five minutes to process the same dataset. The average computational time needed for the method based on least square support vector machine and mean shift algorithm [20] was about 14 minutes. Finally, the method based on beam-hardening collector [19] also needed more than seven minutes to reconstruct the images.

CONCLUSIONS

In this paper a novel metallic artifact approach is introduced in which sinograms of the CT X-ray images are decomposed into illumination and reflectance components by using homomorphic filtering. The sinograms of the artifact-free sections are used as a priori knowledge to initiate the two-step reconstruction algorithm. In the first step, a sequential process is carried out in which the degraded illumination components are substituted with the illumination components of the

closest previous artifact-free sections. At this step, an initial reconstructed sinogram is obtained. The regions in the degraded sinogram with more significant artifacts effect are extracted using a non-linear mask in the second stage. The extracted regions are then combined with the corresponding sinogram which has been achieved using the first step. By transforming back all the reconstructed sinograms to the spatial domain the restored CT image is obtained. The experimental results indicate the efficiency of the proposed metal artifact reduction method in eliminating the streaking artifacts, especially the bright artifacts which are more annoying in practical applications. Using our well-defined weighted reconstruction technique, the important details of the images are preserved as well. Meanwhile, the proposed straight-forward framework does not rely on any additional pre-processing step such as segmentation, smoothing, or background noise reduction.

REFERENCES

1. F. H. Kim, S. P. Moylan, E. J. Garboczi and J. A. Slotwinski, 2017, " Investigation of pore structure in cobalt chrome additively manufactured parts using X-ray computed tomography and three-dimensional image analysis," Additive Manufacturing, vol. 17, pp. 23-38,.
2. S. Ray, V. Kumar, C. Ahuja and N. Khandelwal, 2018, " Computer Aided Automatic Brain Segmentation from Computed Tomography Images using Multilevel Masking," arXiv preprint arXiv*:1809.06215.*,.
3. D. Us, 2013, "Metal Artifact Reduction in Sinograms of Dental Computed Tomography.," Master's thesis of Tampere University of Technology,.
4. K. WA, 2007." X-ray computed tomography," Physics in medicine and biology, vol. 51, no. 13, pp. R29-43,
5. A. Mehranian, M. R. Ay, A. Rahmim and H. Zaidi, 2013, " X-ray CT metal artifact reduction using wavelet domain sparse regularization.," IEEE Transactions on Medical Imaging , vol. 32, pp. 1707-1722.
6. M. Yazdia, L. Gingras and L. Beaulieu, 2005, "An adaptive approach to metal artifact reduction in helical computed tomography for radiation therapy treatment planning: experimental and clinical studies," International Journal of Radiation Oncology,Biology, Physics , vol. 62, pp. 1224-1231.
7. H. Yu, K. Zeng, D. Bharkhada, G. Wang, M. Madsen and O. Saba, 2007, " segmentation-based method for metal artifact reduction," *Academic Radiology*, vol. 14, pp. 495-504.
8. J. Choi, K. Kim, M. Kim, W. Seong and J. Ye, " 2011, Sparsity driven metal part reconstruction for artifact removal in dental CT," Journal of X-ray Science and Technology , vol. 19, pp. 457-475.
9. J. Lim, 1990, Two-dimensional signal and image processing, Englewood Cliffs, NJ, Prentice Hall, 1990, 710 p.
10. R. Gonzalez and R. Woods, 2002, Digital image processing., Prentice hall Upper Saddle River,.
11. Y. Jin, D. Giantsoudi, L. Fu, J. Verburg, L. Gjesteby, G. Wang and B. De Man, 2018, "Metal artifact reduction for radiation therapy: a simulation study," In Medical Imaging 2018: Physics of Medical Imaging , vol. 10573, pp. 105730Q,.
12. D. Wagenaar, E. R. v. d. Graaf, A. v. d. Schaaf and M. J. W. Greuter, 2015, " Quantitative Comparison of Commercial and Non-Commercial Metal Artifact Reduction Techniques in Computed Tomography doi: 10.1371/journal.pone.0127932. eCollection," *PLoS One,* vol. 10, no. 6, p. e0127932.
13. R. Nasirudin, K. Mei, P. Panchev, A. Fehringer, F. Pfeiffer and E. Rummeny, 2015, " Reduction of Metal Artifact in Single Photon-Counting Computed Tomography by Spectral-Driven Iterative Reconstruction Technique," PLoS One , vol. 10, no. 5,.
14. M. Yazdi and M. Mohammadi, 2017, " Metal Artifact Reduction in Dental Computed Tomography Images Based on Sinogram Segmentation Using Curvelet Transform Followed by Hough Transform," Journal of medical signals and sensors, vol. 7, no. 3, pp. 145-152,.
15. M. Abdoli, R. Dierckx and H. Zaidi, 2012, "Metal artifact reduction strategies for improved attenuation correction in hybrid PET/CT imaging," Medical physics, vol. 39, pp. 3343-3360,.
16. H. Park, J. Choi, K. Park, K. Kim, S. Lee and J. Ye, 2013, " Metal artifact reduction in CT by identifying missing data hidden in metals," Journal of X-ray science and technology , vol. 21, pp. 357-372,.
17. C. Peng, B. Qiu, M. Li, Y. Yang, C. Zhang, L. Gong and J. Zheng, 2018, " GPU-Accelerated Dynamic Wavelet Thresholding Algorithm for X-Ray CT Metal Artifact Reduction," IEEE Transactions on Radiation and Plasma Medical Sciences, vol. 2, no. 1, pp. 17-26,.
18. A. De Crop, J. Casselman, T. Van Hoof, M. Dierens, E. Vereecke and N. Bossu, 2015, "Analysis of metal artifact reduction tools for dental

hardware in CT scans of the oral cavity: kVp, iterative reconstruction, dual-energy CT, metal artifact reduction software: does it make a difference?," Neuroradiology, vol. 57, no. 8, pp. 841-849,.

19. H. Park, D. Hwang and J. Seo, 2016, "Metal Artifact Reduction for Polychromatic X-ray CT Based on a Beam-Hardening Corrector," IEEE Transactions on Medical Imaging, vol. 35, no. 2, pp. 38-387.
20. P. Mortaheb and M. Rezaeian, 2016, " Metal Artifact Reduction and Segmentation of Dental Computerized Tomography Images Using Least Square Support Vector Machine and Mean Shift Algorithm," Journal of Medical Signals and Sensors , vol. 6, pp. 1-11,.
21. M. Johari, M. Abdollahzadeh, F. Esmaeili and V. Sakhamanesh, 2018, "Metal Artifact Suppression in Dental Cone Beam Computed Tomography Images Using Image Processing Techniques," Journal of medical signals and sensors, vol. 8, no. 1, pp. 12-24,.
22. E. Meyer, R. Raupach, M. Lell, B. Schmidt and M. Kachelrie, 2010, " Normalized metal artifact reduction (NMAR) in computed tomography.," *Medical physics* , vol. 37, pp. 5482-5493,.
23. H. G. ,. Hassanpour, 2013, "Image Enhancement via Reducing Impairment Effects on Image Components," International Journal of Engineering-Transactions B: Applications , vol. 26, no. 11, pp. 1267-1274,.
24. A. S. M. Kak, 2001, Principles of computerized tomographic imaging, Society for Industrial and Applied Mathematics,.
25. C.-C. Chang and C.-J. Lin, 2011, "LIBSVM: A library for support vector machines.," *ACM Trans. Intell. Syst. Technol.*, vol. 2, no. 3, p. 27,. doi:10.1145/1961189.1961199
26. V. Naranjo Ornedo, R. Llorens Rodriguez, M. Alcaniz Raya and F. Lopez-Mir, 2011, " Metal artifact reduction in dental CT images using polar mathematical morphology," Computer Methods and Programs in Biomedicine, vol. 102, no. 1, pp. 64-74,.
27. X. Yuan, Y. Meng and W. X, 2013, "Illumination Normalization Based on Homomorphic Wavelet Filtering for Face Recognition," Journal of Information Science and Engineering, vol. 29, pp. 579-594,.
28. H. Han, S. Shan, X. Chen and W. Gao, 2008, "Illumination Transfer Using Homomorphic Wavelet Filtering and Its Application to Lighting Insensitive Face Recognition," in IEEE International Conference on Automatic Face and Gesture Recognition, Amsterdam, Netherland,.
29. Turkman, A. 1991, Polymer Application Examples in Industrial Wastewater treatment, New Developments in Industrial Wastewater Treatment, Kluwer Academic Publishers, Dordrecht, The Netherlands, pp. 93-109,.
30. Tzoupanos, N.D. and Zouboulis, A.I. 2008, "Coagulation-flocculation Processes in Water/Wastewater Treatment: The Application of New Generation of Chemical Reagents", *in Proc. 6th IASME/WSEAS* International Conference on Heat Transfer, Thermal Engineering and Environment (THE'08) Rhodes, Greece, pp. 309 – 317.
31. Wilson, F. 1981, Design Calculations in Wastewater Treatment, E. & F. N. Spon Ltd., London, pp. 49 – 68,.

Persian Abstract

DOI: 10.5829/ijee.2018.09.04.06

چکیده

در توموگرافی کامپیوتری اشعه ایکس (CT)، وجود ایمپلنت های فلزی در موضوع ممکن است تصاویر را فاسد کرده و آثار هنری تاریک و روشن را ایجاد کند. در این مقاله یک روش جدید برای کاهش مصنوعی فلز از تصاویر سی تی اسکن دندان ارائه شده است. در روش پیشنهادی، تبدیل رادون به منظور تولید داده های CT در دامنه سینوکس استفاده می شود. سینوژم داده ها را می توان با استفاده از فیلترینگ موجک هوموورفیک به عناصر روشنایی و بازتاب آن تجزیه کرد. بررسی تصاویر CT نشان می دهد که تخریب ناشی از مصنوعات فلزی عمدتا در مولفه روشنایی ظاهر می شود. بنابراین، در رویکرد ما، مولفه روشنایی خراب شده با استفاده از اطلاعات apriori که از بخش های بدون پیشوند قبلی رانده شده است، بازیابی می شود. نتایج نشان داد که آثار فلزی بدون حذف جزئیات مهم تصاویر CT به طور قابل توجهی کاهش می یابد. روش پیشنهادی نیز با سایر روش های موجود در مجموعه ای از تصاویر سی تی اسکن دندان مقایسه شده است. مقایسه ها برتری روش پیشنهادی را نسبت به سایر روش های موجود نشان دادند.